Supporting Information

Experimental section

Chemical and materials

All chemicals used in the experiment were analytical grade, and were used as received without further purification. Bismuth nitrate ($Bi(NO_3)_3 \cdot 5H_2O$), 5,5-Dimethyl-1-Pyrrolidine-N-oxide (DMPO) were purchased from Macklin Reagent Co., Ltd. (Shanghai, China). 2,2,6,6-tetramethylpiperidine (TEMP) was obtained from Dojindo Molecular Technologies, Inc (Japan). Ammonium dihydrogen phosphate ($NH_4H_2PO_4$), ammonium hydroxide ($NH_3 \cdot H_2O$, 25%–28%) and ethanol were purchased from Aladdin (Shanghai, China). Ultra-pure water (Millipore Super Q system, USA) with a resistivity of 18.2 MΩ·cm was used in the experiments.

Catalyst synthesis

The synthesis of the BiOHP pre-catalysts was adopted from previous study (Sahu et al., 2018). Specifically, 4 mmol $Bi(NO_3)_3 \cdot 5H_2O$ are firstly dissolved in 60 mL H_2O in a breaker. After stirring for 10 min, 4 mmol $NH_4H_2PO_4$ is rapidly added and stirred for another 3 h. Subsequently, pH of the mixture is adjusted to 10 by adding a certain amount of concentrated $NH_3 \cdot H_2O$ under vigorously stirring. Finally, the resulting suspension is transferred to a 100 mL Teflon-lined autoclave, sealed and heated at 180℃ for 24 h. The obtained products were separated by centrifugation, washed by deionized water and ethanol for several times, and dried at 60℃ in a vacuum oven.

For synthesis of BiOHP-V_o catalysts, 0.5 g BiOHP pre-catalysts was dispersed into 100 mL H_2O. After a brief ultrasonic, the mixture was irradiated by a 24 W UV light (Cnlight, 254 nm) for 2 h, the irradiation intensity was determined to be 7.3 mW/cm^2. The product was washed with water for several times and dried at 60℃.

The BiOHP-280 photocatalyst is obtained by calcining the BiOHP-V_o catalysts at 280℃ for 0.5 h in the air. The BiOHP-380 photocatalyst is prepared by annealing the BiOHP-V_o catalysts at 380℃ for 2 h.

Materials characterization

Powder X-ray diffraction (XRD) are recorded on a Bruker D8 diffractometer from 5° to 70°. Scanning electron microscopy (SEM) is performed on a Hitachi SU8010 microscope (Japan) at a working voltage of 5 kV. The Fourier transform infrared reflection (FTIR) spectra were obtained using a Thermo Scientific Nicolet iS 50 spectrometer (USA). X-ray photoelectron spectroscopy (XPS) analysis were performed using a Thermo ESCALAB 250Xi (USA) XPS system equipped with a Al Kα source. Thermogravimetry (TG) and differential scanning calorimetry (DSC) was performed using an STA 449 F5 Jupiter synchronous thermal analyzer (NETZSCH, Selb, Germany). Electron paramagnetic resonance (EPR) spectra of oxygen vacancies were obtained from Bruker EMX-PLUS (Germany) spectrometer at low tempreture (77K).

Photodegradation experiments

The photodegradation experiments were conducted using a double-jacketed quartz reactor equipped with a low-pressure Hg UV lamp (Philips, TUV PL-L 18W, 254 nm), the irradiation intensity is determined to be 5.2 mW/cm^2 using a UV-C radiometer (Beijing Normal University, Beijing, China). The reaction tempreture maitanined to be 25℃ by a low-temperature thermostat bath. In a typical experiment, 50 mg catalysts are added into 100 mL PFOA (20 mg/L) solutions. Before irradiation, the mixture was stirred for 30 min in darkness to achieve an adsorption-desorption equilibrium. Subsequently, UV light is turned on to initiate the degradation reaction. The pH of the solution was measured to be 4.5 without adjustment. At a given intervals, 2 mL of the suspension was taken out. Then the resulting supernatant was centrifuged and filtered by a 0.22 μm polyethersulfone (PES) membrane for analysis.

Analytical methods

The concentration of PFOA was quantified by high performance liquid chromatography (HPLC) (Shimadzu-20 A, Japan) equipped with an Eclipse XDB-C18 column (4.6 I.D.×150 mm, 5 μm). 0.1 wt% H_3PO_4 (mobile phase A) and acetonitrile (mobile phase B) (50:50, 0.9 mL/min) were used as the mobile phases for HPLC analysis. The detection wavelength was set as 210 nm, and the column temperature is 40℃.

DMPO was used as trapping agent to detect the generation of •OH and $•O_2^-$ while TEMP was employed to analyze the production of $^1O_2$.

The concentrations of fluorine ions were measured by an ion Chromatography (Thermo Fisher Scientific, USA).

Defluorination efficiency of PFOA was calculated as follow (Eq. (S1)):

$$\text{Defluorination efficiency} = \frac{C_{t(F^-)}}{15\times C_0}\times 100\% \quad , \qquad \text{(S1)}$$

where $C_{t(F^-)}$ is the concentration of fluoride ion during the different photodegradation intervals, C_0 is the initial concentration of PFOA, and the factor 15 corresponds to the number of fluorine atoms in one PFOA molecule.

Table S1 Surface area and pore analysis of catalysts.

Samples	BET Surface Area (m^2/g)	Pore size (nm)
BiOHP-V_o	1.647	9.7
BiOHP-280	1.582	9.1
BiOHP-380	1.579	10.3

Table S2 Comparison of degradation and defluorination efficiency of PFOA by different photocatalysts.

Catalyst	Light	Reaction conditions	Reaction time	Degradation & Defluorination efficiency	Ref.
$TiO_2/H_2C_2O_4$	254 nm, 23 W	N_2 atmosphere C_0 = 10 mg/L $C_{cat.}$= 0.5 g/L	3 h	86.7% & 16.5%	(Wang et al., 2011)
TiO_2/O_3	254 nm, 28 W	C_0 = 10 mg/L $C_{cat.}$= 0.2 g/L O_3 = 25 mg/h	4 h	99.1% & 44.3%	(Huang et al., 2016)
β-Ga_2O_3	254 nm, 50 W	N_2 atmosphere C_0 = 10 mg/L $C_{cat.}$= 0.5 g/L	1.5 h	100% & 56%	(Zhao et al., 2015)
In_2O_3	254 nm, 23 W	O_2 atmosphere C_0 = 10 mg/L $C_{cat.}$= 0.5 g/L	4 h	80% & 33.1%	(Li et al., 2012)
MnO_x-In_2O_3	Xenon lamp, 500 W	C_0 = 50 mg/L $C_{cat.}$= 0.5 g/L	4 h	100% & 3%	(Wu et al., 2019)
BiOCl	254 nm, 10 W	C_0 = 8.28 mg/L $C_{cat.}$= 0.5 g/L	12 h	100% & 59.3%	(Song et al., 2017)
Defective BiOCl	Xenon lamp, 300 W	C_0 = 20.7 mg/L $C_{cat.}$= 0.5 g/L	8.5 h	68.8% & 12.86%	(Sun et al., 2019)
BN	254 nm, 24 W	C_0 = 50 mg/L $C_{cat.}$= 2.5 g/L	4 h	> 99% & 52%	(Duan et al., 2020)

BiOHP/CS	254 nm, 18 W	C_0 = 200 μg/L $C_{cat.}$ = 1.0 g/L	4 h	> 99% & 32.5%	(Xu et al., 2020)
BiOHP-V_o	254 nm, 18 W	C_0 = 20 mg/L $C_{cat.}$ = 0.5 g/L	3 h	>99% & 57.6%	This work

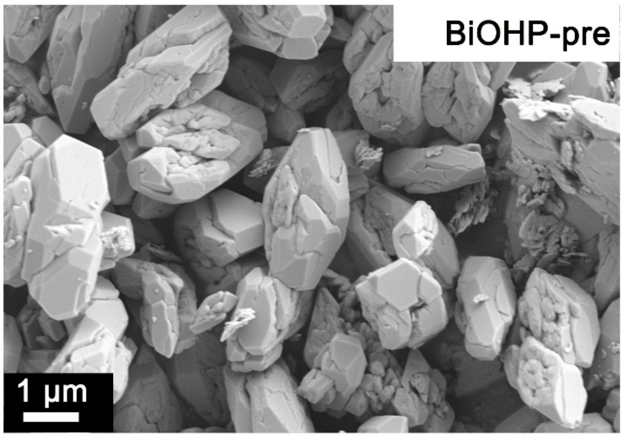

Fig. S1 SEM image of the BiOHP pre-catalysts.

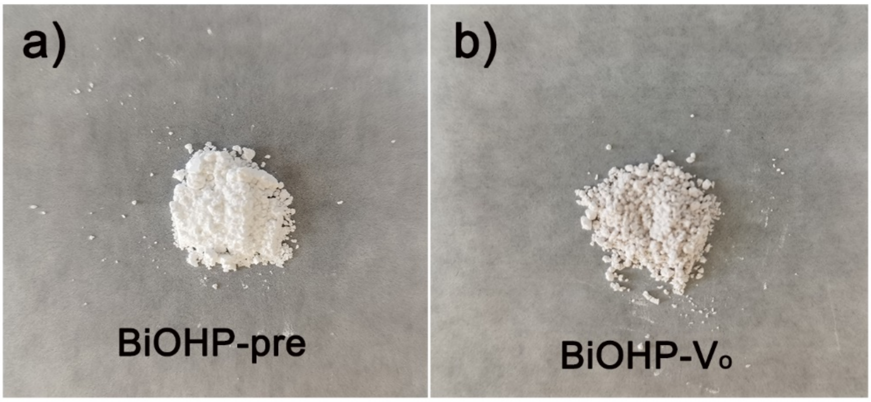

Fig. S2 Photos of the (a) BiOHP-pre and (b) BiOHP-V_o catalysts.

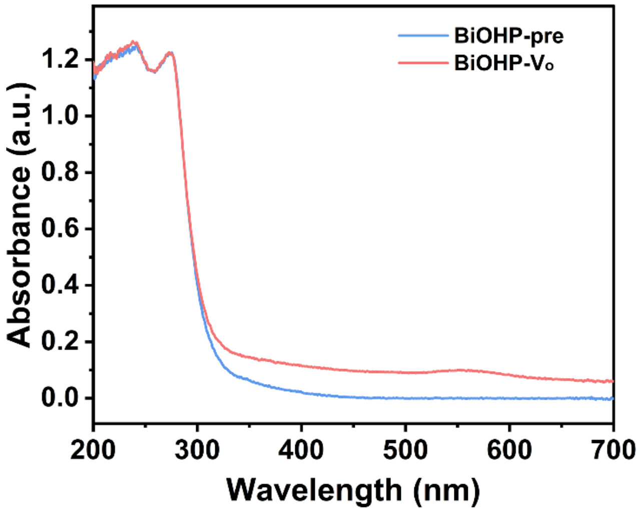

Fig. S3 UV-vis DRS of as prepared BiOHP-pre and BiOHP-V_o catalysts.

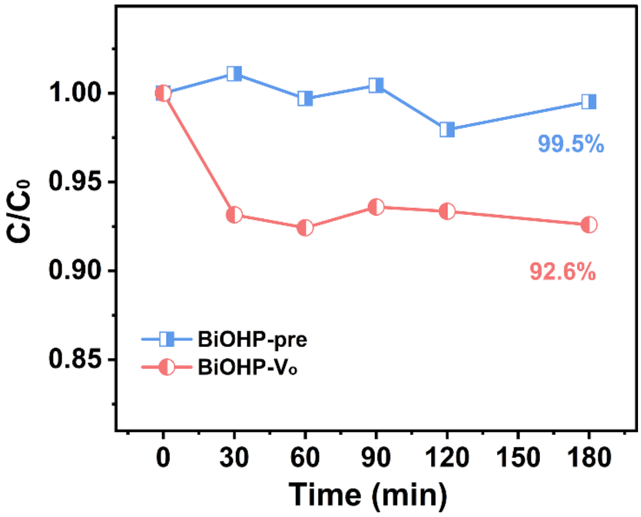

Fig. S4 Adsorption experiments of PFOA by BiOHP-pre and BiOHP-V_o.

Reaction condition: 0.5 g/L catalysts, 20 mg/L PFOA.

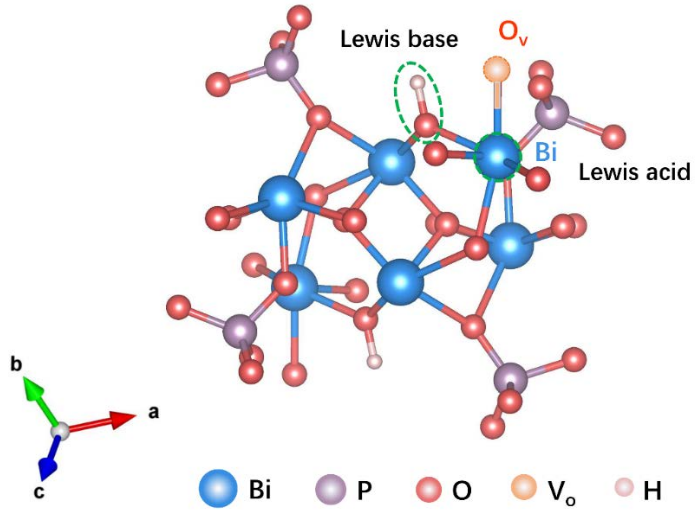

Fig. S5 Structure of surface frustrated Lewis pairs in BiOHP-V_o.

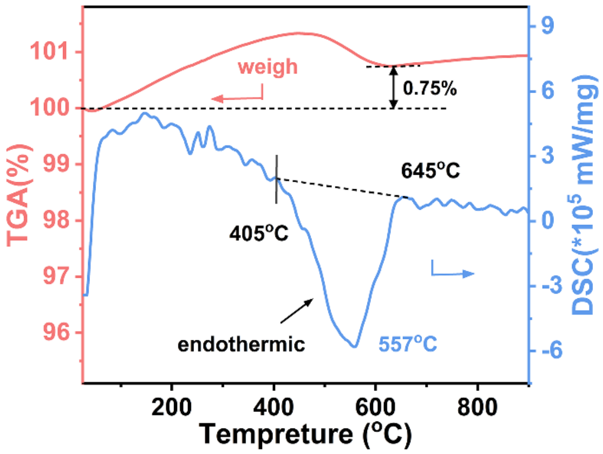

Fig. S6 TG-DSC analysis of BiOHP-V_o catalysts.

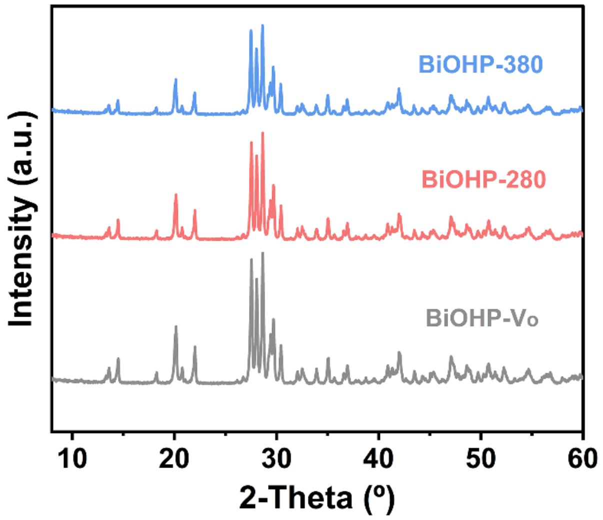

Fig. S7 XRD patterns of BiOHP-V_o, BiOHP-280, and BiOHP-380.

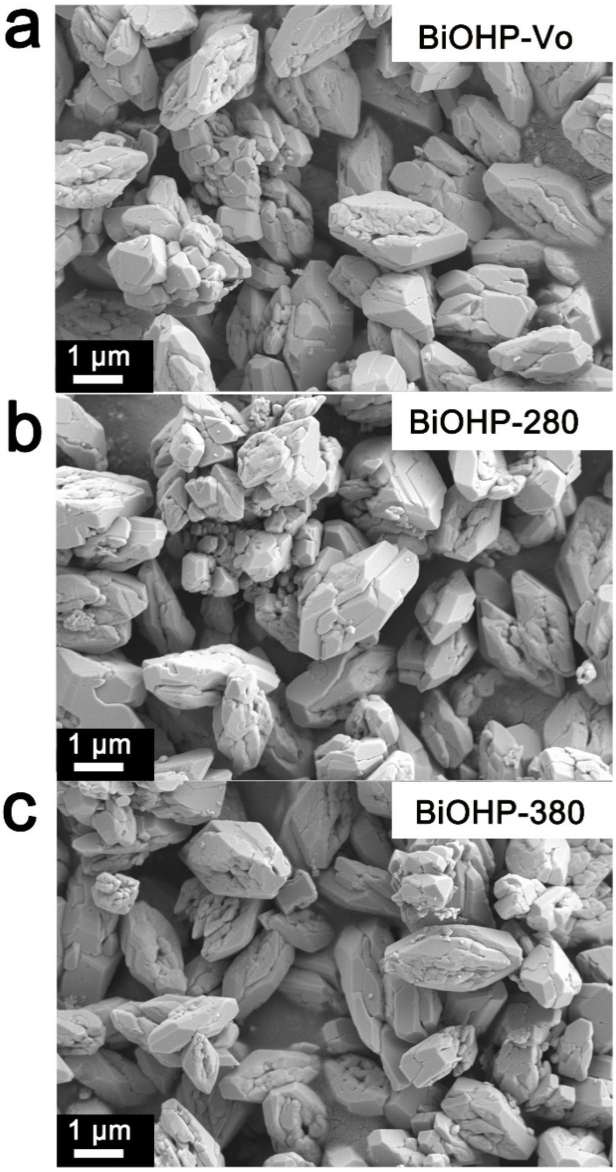

Fig. S8 SEM images of the (a) BiOHP-V$_o$, (b) BiOHP-280, and (c) BiOHP-380 catalysts.

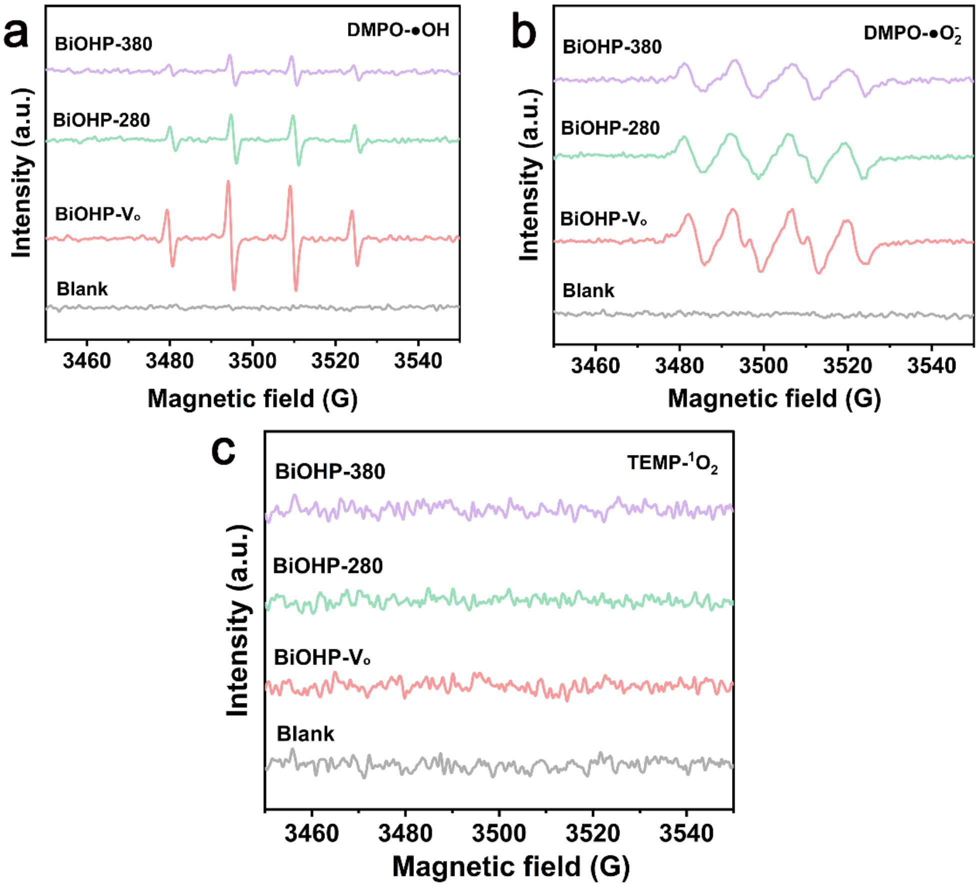

Fig. S9 EPR spectra of (a) DMPO-•OH, (b) DMPO-•O_2^- and (c) TEMP-$^1O_2$ by different catalysts. ([DMPO]$_0$ = 80 mM, [TEMP]$_0$ = 100 mM).

As shown in Fig. S9, both •OH and •O_2^- were detected in the BiOHP photocatalytic systems. In particular, BiOHP-V$_o$ could generate more ROS, suggesting the contribution of SFLP to the improved oxidative capacity, leading to a superior degradation efficiency.

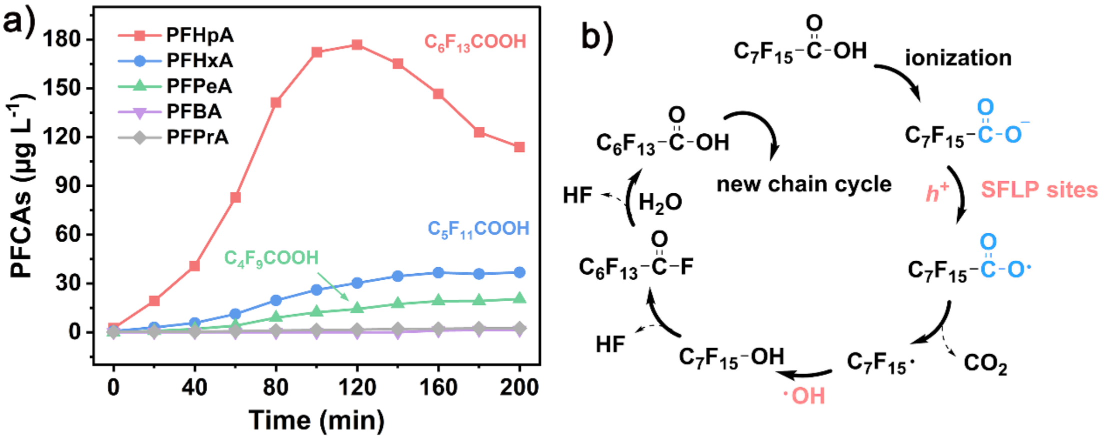

Fig. S10 (a) Time-dependent concentration changes of intermediates during PFOA photodegradation by BiOHP-V$_o$ catalysts. (b) PFOA degradation pathways by SFLPs catalysts.

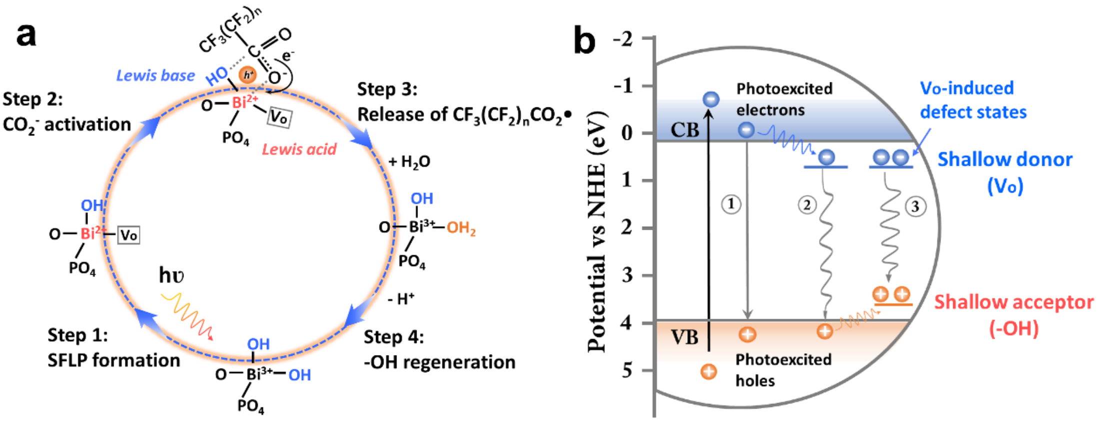

Fig. S11 (a) Proposed activation mechanism of carboxyl in PFOA oxidation over SFLPs catalyst. (b) Scheme illustration of charge transfer pathways in the presence of SFLPs.

References

Duan L, Wang B, Heck K, Guo S, Clark C A, Arredondo J, Wang M, Senftle T P, Westerhoff P, Wen X, Song Y, Wong M S (2020). Efficient photocatalytic PFOA degradation over boron nitride. Environmental Science & Technology Letters, 7(8): 613–619

Huang J, Wang X, Pan Z, Li X, Ling Y, Li L (2016). Efficient degradation of perfluorooctanoic acid (PFOA) by photocatalytic ozonation. Chemical Engineering Journal, 296: 329–334

Li X, Zhang P, Jin L, Shao T, Li Z, Cao J (2012). Efficient photocatalytic decomposition of perfluorooctanoic acid by indium oxide and its mechanism. Environmental Science & Technology, 46(10): 5528–5534

Sahu S P, Qanbarzadeh M, Ateia M, Torkzadeh H, Maroli A S, Cates E L (2018). Rapid degradation and mineralization of perfluorooctanoic acid by a new petitjeanite $Bi_3O(OH)(PO_4)_2$ microparticle ultraviolet photocatalyst. Environmental Science & Technology Letters, 5(8): 533–538

Song Z, Dong X, Wang N, Zhu L, Luo Z, Fang J, Xiong C (2017). Efficient photocatalytic defluorination of perfluorooctanoic acid over BiOCl nanosheets via a hole direct oxidation mechanism. Chemical Engineering Journal, 317: 925–934

Sun Y, Li G, Wang W, Gu W, Wong P K, An T (2019). Photocatalytic defluorination of perfluorooctanoic acid by surface defective BiOCl: Fast microwave solvothermal synthesis and photocatalytic mechanisms. Journal of Environmental Sciences-China, 84: 69–79

Wang Y, Zhang P (2011). Photocatalytic decomposition of perfluorooctanoic acid (PFOA) by TiO_2 in the presence of oxalic acid. Journal of Hazardous Materials, 192(3): 1869–1875

Wu Y, Li Y, Fang C, Li C (2019). Highly efficient degradation of perfluorooctanoic acid over a MnO_x-modified oxygen-vacancy-rich In_2O_3 photocatalyst. ChemCatChem, 11(9): 2297–2303

Xu T, Zhu Y, Duan J, Xia Y, Tong T, Zhang L, Zhao D (2020). Enhanced photocatalytic degradation of perfluorooctanoic acid using carbon-modified bismuth phosphate composite: effectiveness, material synergy and roles of carbon. Chemical Engineering Journal, 395: 124991

Zhao B, Li X, Yang L, Wang F, Li J, Xia W, Li W, Zhou L, Zhao C (2015). ß-Ga_2O_3 nanorod synthesis with a one-step microwave irradiation hydrothermal method and its efficient photocatalytic degradation for perfluorooctanoic acid. Photochemistry and Photobiology, 91(1): 42–47